Ultrafast time-resolved spectroscopy of In_2O_3 nanowires

Demetra Tsokkou,[1] Andreas Othonos,[1,a)] and Matthew Zervos[2]
[1]*Department of Physics, Research Center of Ultrafast Science, University of Cyprus, P.O. Box 20537, Nicosia 1678, Cyprus*
[2]*Department of Mechanical Engineering, Nanostructured Materials and Devices Laboratory, University of Cyprus, P.O. Box 20537, Nicosia 1678, Cyprus*

(Received 27 August 2009; accepted 13 September 2009; published online 21 October 2009)

Ultrafast carrier dynamics in In_2O_3 nanowires with an average diameter of $\approx 100 \pm 20$ nm grown by the vapor-liquid-solid method have been investigated in detail using differential absorption spectroscopy with femtosecond resolution. Measurements revealed that state filling is important for states above the band gap and states just below the band edge, thus demonstrating the critical role that shallow traps play in the relaxation of the photogenerated carriers. Furthermore, time-resolved intensity measurements revealed the importance of Auger recombination in the relaxation of carriers in the In_2O_3 nanowires and provided the maximum fluence (~ 3 $\mu J/cm^2$) where this recombination mechanism may be considered negligible. Transient measurements in this low-fluence regime for carriers above the band gap revealed single exponential recovery (~ 1.5 ns) associated with recombination of the photogenerated carriers. Similar behavior has been observed for the photogenerated carriers distributed within the shallow traps just below the band edge. Furthermore, measurements at longer probing wavelengths provided an estimate of the nonradiative relaxation of carriers (~ 300 ps), which are distributed among the midgap states. Finally, long-lived oscillations in the transient reflection were detected, which corresponds to the presence of longitudinal acoustic phonons in the In_2O_3 nanowires. © *2009 American Institute of Physics*. [doi:10.1063/1.3245339]

I. INTRODUCTION

Indium oxide (In_2O_3) is an important, *n*-type semiconductor oxide,[1] due to its large band gap, i.e., $E_G = 3.5-3.75$ eV and has been utilized for applications in electronic and optoelectronic devices, such as window heaters, flat planet displays, solar cells, and organic light emitting diodes.[2–4] In addition, In_2O_3 nanowires (NWs) are suitable candidates for gas sensors and the detection of toxic gases such as NO_2, NO, and NH_3 (Refs. 5–7) due to the enhanced surface-to-volume ratio but also as field effect transistors.[8] Furthermore In_2O_3 NWs grown by the vapor-liquid-solid (VLS) mechanism can be readily integrated with mainstream Si devices since the issue of lattice mismatch is not so critical; i.e., NWs can be grown with relative ease by the VLS mechanism on a large variety of substrates. Consequently, in addition to quantum confinement, their electronic and optoelectronic properties are expected to be also dependent on the surfaces states and properties. Previous investigations of photoluminescence in nonintentionally doped In_2O_3 NWs have revealed peaks with energies below the band gap,[9–12] which are associated with oxygen defect states, such as vacancies and antisites. However, there has been no detailed investigation using ultrafast time-resolved spectroscopy which can provide a more detailed understanding of the nature of the electronic states in In_2O_3 NWs and other important physical properties. Consequently, we have undertaken a detailed investigation of the carrier dynamics and relaxation mechanisms in In_2O_3 NWs that were grown by chemical vapor deposition (CVD). We find that the relaxation times of carriers excited into the conduction band (CB) are similar to those in shallow, defect related states, which are energetically situated just below the CB edge. In contrast, we find that midgap states have a different temporal behavior, while long-lived oscillations in the reflection were also detected due to longitudinal phonons. These findings are discussed in detail in addition to extracting relaxation times and the velocity of sound in In_2O_3 NWs.

II. EXPERIMENTAL PROCEDURE

Indium oxide NWs were prepared using an atmospheric pressure CVD reactor consisting of four mass flow controllers (MFCs) and a horizontal quartz tube furnace, capable of reaching a maximum temperature of 1100 °C. High purity indium powder (Aldrich, Mesh −100, 99.99%) was used and about ≈0.2 g was weighed and loaded into a quartz boat. In_2O_3 NWs were grown on n^+ Si(111) substrates that were coated with 0.5 nm of Au which was deposited on Si(111) via sputtering at a slow rate using an Ar plasma under a pressure $<10^{-4}$ mbar. After loading the In powder and Au/Si(111) samples into the quartz boat, it was inserted into the reactor and positioned directly above the thermocouple used to measure the heater temperature.

Initially, oxygen was admitted into the reactor at a flow of 50 SCCM (SCCM denotes cubic centimeter per minute at STP) for 10 min at room temperature (RT). Following this the O_2 flow was terminated and argon (Ar) was introduced at 500 SCCM for 10 min after which the temperature was increased up to 700 °C, using a ramp rate of 30 °C/min. During growth the temperature and flow of Ar were maintained constant at 700 °C and 100 SCCM, respectively, for 90 min.

a)Electronic mail: othonos@ucy.ac.cy.

 © 2009 American Institute of Physics

Downloaded 30 May 2010 to 194.42.23.188. Redistribution subject to AIP license or copyright; see http://jap.aip.org/jap/copyright.jsp

Finally, upon cooling down the flow of Ar was maintained at 100 SCCM and the sample was removed from the reactor only after cooling down to RT. Upon visual inspection, the surface of the sample had a light-blue color, while the In powder, which melts at 157 °C always formed a graylike, spherical drop. For the purpose of ultrafast spectroscopy, In_2O_3 NWs were grown directly on quartz which was also coated with ≈0.5 nm of Au.

The morphology of the In_2O_3 NWs was examined with a Tescan scanning electron microscope (SEM) while the crystal structure and the phase purity of the NWs were investigated using a Shimadzu, XRD-6000, x-ray diffractometer and Cu $K\alpha$ source. A scan of θ-2θ in the range between 20° and 80° was performed for the In_2O_3 NWs that were grown on Si(111) and quartz. Following this the optical transmission spectrum was obtained by a standard UV/visible spectrometer (Perkin Elmer Lambda 950). Furthermore, transient nondegenerate absorption spectroscopy was performed using a typical supercontinuum pump-probe configuration.[13] The initial femtosecond laser source used in the experiment was a self-mode-locked Ti:sapphire oscillator generating 45 fs, 5 nJ pulses at 790 nm with a repetition rate of 100 MHz. These pulses were amplified $\sim 10^6$ times in a typical regenerative amplifier system producing 45 fs pulses at a repetition rate of 5 kHz. Part of the output energy was then directed into an optical parametric amplifier generating femtosecond pulses in the UV spectral region. A small part of the fundamental energy was also used to generate a supercontinuum white light by focusing on a thin sapphire plate. Two such setups were utilized in order to broaden the range of selected probing wavelengths. The first setup is used to generate the continuum white light in the region between 400 and 1000 nm, while the second one produces wavelengths in ultraviolet region between 300 and 400 nm, by using an additional second harmonic crystal. The desired probing wavelength was selected by using a band-pass filter and transmission and reflection changes were detected by Si detectors.

III. RESULTS AND DISCUSSION

Indium oxide NWs have been grown by a variety of methods including CVD via carbothermal reduction of In_2O_3 and active carbon at 980 °C,[14] direct oxidation of In under high temperatures (≥1000 °C) [10,15,16] and thermal evaporation of In, in the presence of H_2O vapor at 850 °C and a flow of 50 SCCM Ar.[17] Moreover, Zhang *et al.*[18] synthesized In_2O_3 NWs by using hydrogen and Ag as a catalyst. In addition, In_2O_3 NWs have been grown by annealing of Au/In films at 400 °C.[19,20] A typical SEM image of the In_2O_3 NWs, grown at 700 °C directly on the Au coated quartz substrate, is shown in Fig. 1. A high density of In_2O_3 NWs is clearly apparent and the NWs have an average diameter of $\approx 100 \pm 20$ nm and lengths up to few micrometers, as can be seen from Fig. 1. It should be pointed out that the diameter of the NWs is not uniform along their length and they are tapered at their edges.

The In_2O_3 NWs grown at T_G=700 °C on silicon and quartz are characterized by intense reflection peaks corresponding to the (2 1 1), (2 2 2), (4 1 1), (4 0 0), (4 4 0), and

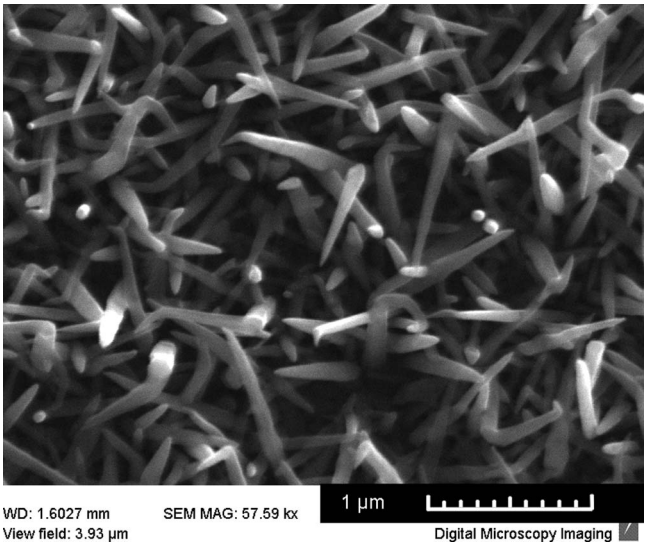

FIG. 1. SEM images of the In_2O_3 NWs grown at 700 °C on 0.5 nm Au/quartz.

(6 2 2) crystallographic planes of In_2O_3 having the cubic bixbyite structure, also called C type rare earth oxide structure with a lattice constant a=10.11 Å.[18] No NWs were obtained on plain Si (111), suggesting that the In_2O_3 NWs grow by the VLS mechanism as has been also reported by other groups.[10,18,20] In addition, no deposition occurred for temperatures lower than T_G=700 °C due to the formation of an oxide shell around the molten indium upstream, which reduces the vapor pressure of indium inside the reactor, even though O_2 was always admitted at the very beginning of the process and RT. This is also consistent with the fact that no In_2O_3 NWs were obtained for $T \leq 900$ °C under a flow of O_2 during growth, which leads to the formation of an even thicker oxide shell surrounding the molten In upstream (Fig. 2). For $T > 900$ °C, the expanding In melt is known to break open the oxide shell, releasing In which then reacts directly with O_2 and leads to the formation of a large density of octahedral In_2O_3 nanocrystals with an average diameter of 500 nm, as described in detail elsewhere.[21] Consequently, oxidation of In under a flow of O_2 during growth does not lead to the formation of In_2O_3 NWs and so it is essential that the O_2 level is maintained low which is consistent with the use of 5% H_2 in the growth of In_2O_3 NWs by Zhang *et al.*[18]

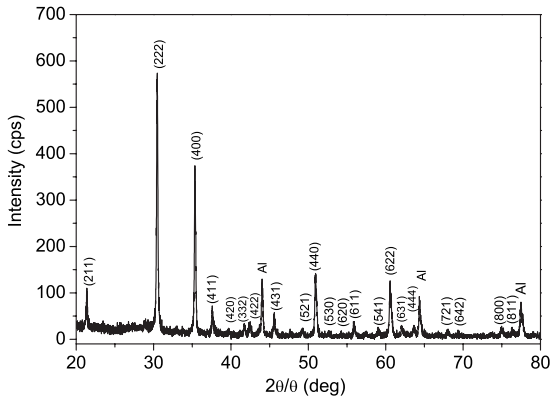

FIG. 2. X-ray diffraction pattern of the In_2O_3 NWs grown on quartz.

Downloaded 30 May 2010 to 194.42.23.188. Redistribution subject to AIP license or copyright; see http://jap.aip.org/jap/copyright.jsp

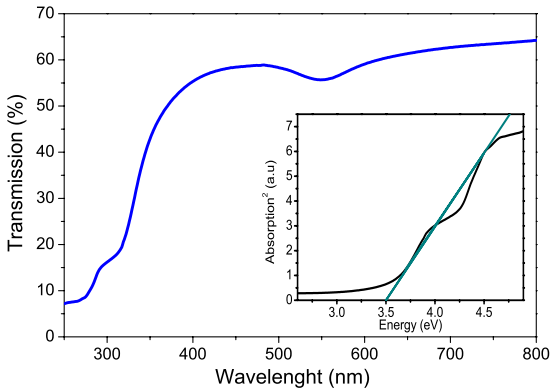

FIG. 3. (Color online) Optical transmission spectrum of In_2O_3 NWs on quartz. The inset shows the square of the absorption vs the energy providing an estimate for the bandgap of the In_2O_3 NWs.

Steady state transmission measurements were carried out following the growth of the In_2O_3 NWs and are shown in Fig. 3. The inset of Fig. 3 is a plot of the absorption squared versus the photon energy providing an estimate of the energy gap of the In_2O_3 NWs, which is $\approx$3.5 eV ($\equiv$354 nm). Following this, time-resolved absorption measurements using optical excitation at 320 nm and different probing wavelengths were carried out and shown in Fig. 4. The estimated absorbed pump fluence was approximately 575 $\mu J/cm^2$. Looking at the experimental data, we notice a positive or negative change in the absorption depending on the probing wavelength. Generally, an initial fast increase, or decrease, is observed in the absorption that is followed by a much longer recovery. A negative change in absorption is observed for probing wavelengths below 410 nm and within the spectral region of 520–550 nm. We should point out that the recovery of absorption is quite different between the two regions; specifically in the visible probing region, the recovery is much faster than the respective recovery in the UV probing region. On the other hand, a positive change is recorded between 430–500 and 600–980 nm. This positive change in the photoinduced absorption is a result of carrier re-excitation to higher energy states by the probing pulses and is dependent

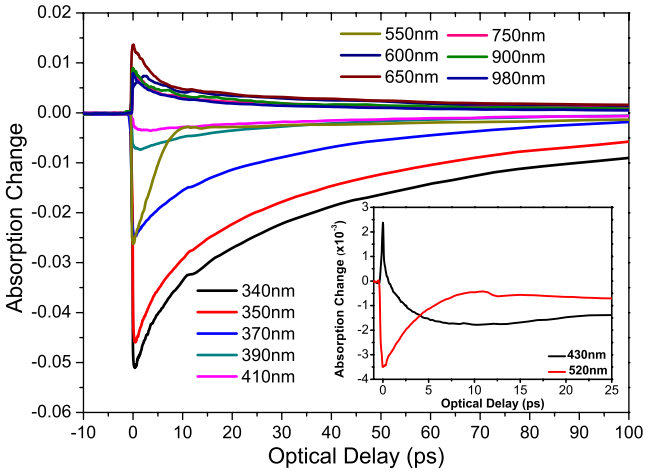

FIG. 4. (Color online) Nondegenerate, time-resolved, transient absorption measurements of the In_2O_3 NWs using ultrafast excitation pulses at 320 nm and probing pulses in the range of 340–980 nm.

on the number of carriers present in the probing energy states and the coupling efficiency between the initial and final states. The observed negative change in the absorption is attributed to state filling, which is due to the occupation of energy states by photogenerated carriers. In most cases both effects are present, while the sign is determined by the dominant effect and the temporal evolution reflects carrier relaxation out of the probing states.

Above band gap excitation ($\lambda > 320$ nm) will result in the generation of electrons (holes) in the conduction (valence) band. These photogenerated carriers will occupy states, resulting in state filling. This is the dominant effect for probing wavelengths corresponding to energies larger than the band gap. The same behavior with similar relaxation times is also observed for probing wavelengths corresponding to energies just below the band edge. These are attributed to additional energy states that are located below the CB edge and are associated with oxygen defects in the In_2O_3 NWs. This is in agreement with previous reports,[9–12] which suggest that oxygen vacancies are formed due to incomplete oxidation during growth and act as donors resulting in additional states below the CB edge. In addition, indium interstitials, as in the case of In_2O_3 octahedrons,[22] may also be a contributing factor to the presence of energy states within the band gap. A more complicated behavior is observed at 430 nm. Initially, free carrier absorption is observed for times near the zero optical delay, while state filling becomes evident for longer times, as shown in the inset of Fig. 4. This behavior is attributed to free carrier absorption from energy states near the excitation region to higher energy states and results in a positive change in absorption. However, as carriers relax into the probing states below the band edge, state filling effects become evident and clearly dominate for longer times.

Here we should point out that a different behavior is observed in the narrow probing region of 520–550 nm, where state filling is apparent, due to the surface plasmon resonance of the Au which is required for the formation of In_2O_3 NWs. This plasmon resonance is due to the electron interaction with the electromagnetic field, associated with intraband and interband transitions of conduction electrons between 5*d* and 6*s* orbitals.[23–25] In order to confirm this, we repeated the experiment using only 0.5 nm Au on quartz observing the same behavior, in the region between 520 and 600 nm. No signal was detected in other regions. The presence of the surface plasmon resonance in this region is also supported by the steady state transmission measurements. This effect induces an extra reduction in the transmission signal as observed in the region between 520 and 600 nm, as shown in Fig. 3.

It is clearly evident from the transient absorption measurements that free carrier absorption is the dominant effect following ultrafast pulse excitation when probing in the IR spectral region. A delay in reaching maximum signal is noted when probing at 600 nm. This is a result of the simultaneous existence of state filling effect, due to the plasmon resonance and free carrier absorption from the In_2O_3 NWs. Apart from this minor difference at 600 nm, it appears that the carrier relaxation is the same at all longer probing wavelengths, sug-

Downloaded 30 May 2010 to 194.42.23.188. Redistribution subject to AIP license or copyright; see http://jap.aip.org/jap/copyright.jsp

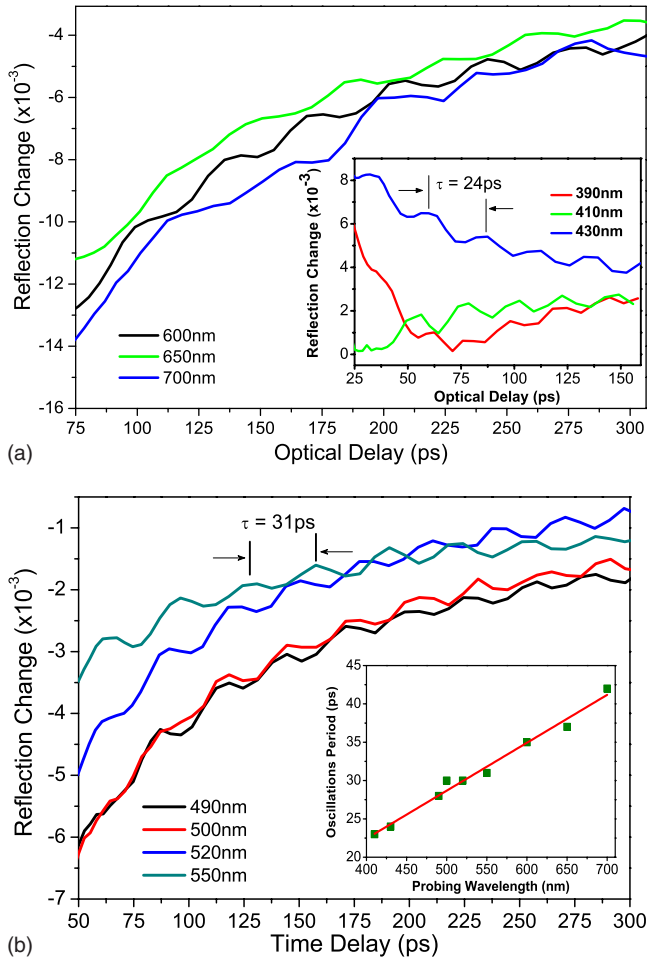

FIG. 5. (Color online) Reflection change is shown for times greater than 50 ps and probing wavelengths between (a) 600–700 and 390–430 nm, in the inset of Fig. 5(a), and (b) 490–550 nm. The period of oscillations is presented in the inset of Fig. 5(b) as a function of probing wavelength.

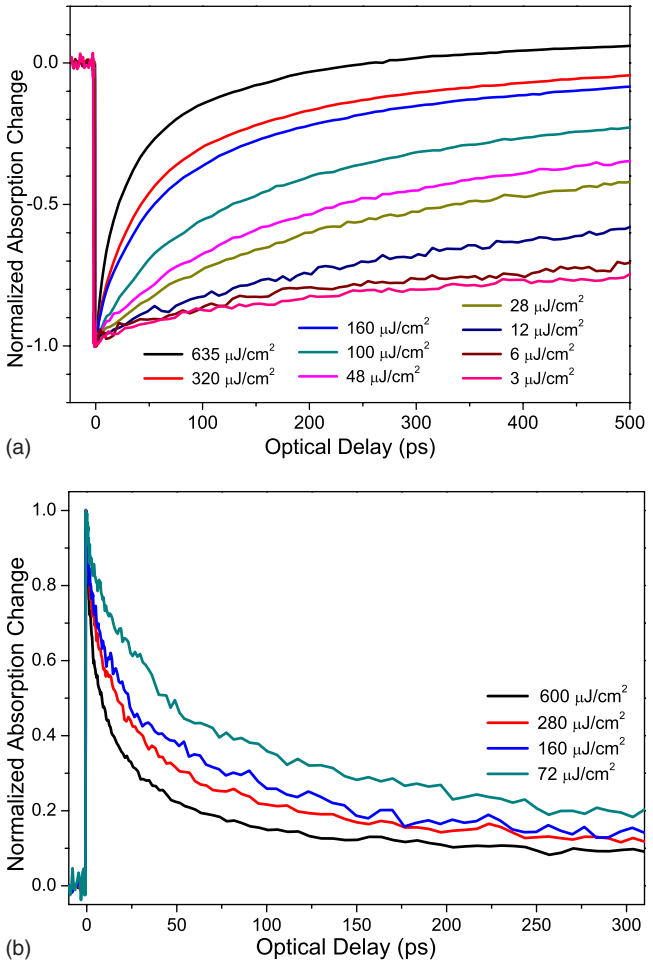

FIG. 6. (Color online) Time resolved transient normalized absorption measurements of the In_2O_3 NWs on quartz using ultrafast UV excitation pumping pulses at 320 nm and probing pulses at (a) 350 nm and (b) 980 nm for different absorbed fluences.

gesting that the same kind of states are probed. We believe that these probed states are not states in the CB or states located just below the CB edge due to the different temporal behaviors between the two regions, at the specified pump fluence. This conclusion is further supported by intensity measurements that are discussed in detail below, supporting that the probed states are midgap states.

A closer look at the transient absorption measurements for probing wavelengths greater than 390 nm depicts an interesting oscillatory behavior, as shown in Figs. 5(a) and 5(b). Long-lived oscillations are observed in the differential reflectivity following a few tens of picoseconds from the initial excitation. A plot of the period of oscillations versus the probing wavelength, shown in the inset of Fig. 5(b), suggests a linear dependence.

We believe that the observed oscillations are associated with coherent acoustic phonons[26,27] generated at the Au nanoparticles and lunged into the In_2O_3 NWs. This wave modifies the local dielectric constants and creates a discontinuity. When the probe pulse is incident onto the sample, part of the light is reflected from the discontinuity of the dielectric constant and the rest of the transmitted light reaches the Au interface where it gets reflected. Therefore as these acoustic phonons travel along the axis of the NWs, the Au surface and the strain wave surface act as an interferometer. Oscillations arise from the fact that the distance between the two surfaces is constantly changing with time, causing a periodic phase difference between the two reflected beams. A linear fit of the period of oscillation versus the probing wavelength was performed based on the equation given by Thomsen *et al.*:[28]

$$\tau = \lambda/(2nv_s \cos\theta), \quad (1)$$

where λ is the probing wavelength, n is the refraction index, which is equal to $n=1.98$ at 500 nm in the case of In_2O_3,[29] v_s is the sound velocity in the material, and θ is the angle between probe pulse and the normal to the sample. This fit gave an estimate of the sound velocity in indium oxide to be approximately $v_s=(4.1\pm0.5)\times10^5$ cm/s.

To further improve our understanding of the carrier relaxation mechanism in this material, transient absorption measurements were performed at different excitation fluences. Normalized transient absorption measurements at probing wavelengths of 350 and 980 nm are shown in Figs. 6(a) and 6(b), respectively. In both cases, carrier relaxation becomes faster as the carrier concentration increases, suggesting that Auger recombination is a contributing factor in the dynamics at the fluence used in this work. For the smaller

Downloaded 30 May 2010 to 194.42.23.188. Redistribution subject to AIP license or copyright; see http://jap.aip.org/jap/copyright.jsp

probing wavelengths (350 nm), Auger recombination appears to play a significant role in the relaxation of the carriers. This effect diminishes with decreasing intensity and considered negligible for energies smaller than 3 $\mu J/cm^2$. At such low intensities, a single exponential recovery is observed with a time constant of 1.5 ns. Here we should point out that intensity measurements at probing wavelengths of 370 and 390 nm depict similar temporal behavior. The data in Fig. 6(b) clearly show that free carrier absorption is the main contributing factor for a probing wavelength equal to 980 nm. Furthermore, the temporal behavior is different from that seen when probing above the band gap. This suggests that we are actually probing within the band gap and most likely the midgap states. This is further supported by the fact that Auger recombination is less pronounced [see Fig. 6(b)] at the same fluence than when probing at 350 nm which is attributed to the distribution of the photogenerated carriers in the large number of states below the band edge. Measurements at the lowest fluence shown in Fig. 6(b) depict a fast relaxation time constant of 26 ps which is attributed to transitions between surface/defect states. In addition, a slow relaxation time is also present which is of the order of hundreds of picoseconds ($\approx$300 ps) attributed to nonradiative recombination.

IV. CONCLUSIONS

Ultrafast carrier dynamics in In_2O_3 NWs following the excitation above the direct band gap was investigated in detail. Steady state transmission measurements provided an estimate of the energy gap of these NWs to be 3.5 eV. Transient absorption measurements revealed that state filling is the dominant effect for states above the CB edge, as well as for states residing below the CB edge demonstrating the importance of shallow traps (associated with defect states) in the relaxation of photogenerated carriers. Furthermore, time-resolved intensity measurements revealed the important role that Auger recombination plays in the relaxation of ultrafast photogenerated carriers and provided the maximum fluence (3 $\mu J/cm^2$) where Auger recombination may be considered negligible. Transient measurements in this low-fluence regime for carriers above the band gap revealed single exponential recovery of the order of $\sim$1.5 ns associated with recombination of the photogenerated carriers. Similar behavior has also been observed for the photogenerated carriers distributed within the shallow traps just below the band edge. Furthermore, measurements at longer probing wavelengths provided an estimate of the nonradiative relaxation of carriers ($\sim$300 ps) which are distributed among the midgap states. Furthermore, time-resolved measurements revealed an oscillatory behavior in the reflection signal for probing wavelengths longer than 390 nm. This behavior is attributed to acoustic phonons which provided an estimate of the sound velocity in In_2O_3 NWs to be $v_s=(4.1\pm0.5)\times10^5$ cm/s.

ACKNOWLEDGMENTS

The work in this article was supported by the Research Promotion Foundation of Cyprus under Grant Nos. EPYNE/0504/06, EPYNE/0506/02, EPYAN/0506/04, and BE0308/03 for fundamental research in the area of nanotechnology and nanomaterials.

[1] O. N. Mryasov and A. J. Freeman, Phys. Rev. B **64**, 233111 (2001).
[2] C. G. Granqvist, Appl. Phys. A: Mater. Sci. Process. **57**, 19 (1993).
[3] H. Kobayashi, T. Ishiba, Y. Nakato, and H. Mori, J. Appl. Phys. **78**, 3931 (1995).
[4] J. S. Kim, R. H. Friend, and F. Cacialli, Appl. Phys. Lett. **74**, 3084 (1999).
[5] C. S. Rout, K. Ganesh, A. Govindaraj, and C. N. R. Rao, Appl. Phys. A: Mater. Sci. Process. **85**, 241 (2006).
[6] D. Zhang, C. Li, X. Liu, S. Han, T. Tang, and C. Zhou, Appl. Phys. Lett. **83**, 1845 (2003).
[7] D. Zhang, Z. Liu, C. Li, T. Tang, X. Liu, S. Han, B. Lei, and C. Zhou, Nano Lett. **4**, 1919 (2004).
[8] D. Zhang, C. Li, S. Han, X. Liu, T. Tang, W. Jin, and C. Zhou, Appl. Phys. Lett. **82**, 112 (2003).
[9] F. Zeng, X. Zhang, J. Wang, L. Wang, and L. Zhang, Nanotechnology **15**, 596 (2004).
[10] S. Kar and S. Chaudhuri, Chem. Phys. Lett. **422**, 424 (2006).
[11] M. Mazzera, M. Zha, D. Calestani, A. Zappettini, L. Lazzarini, G. Salviati, and L. Zanotti, Nanotechnology **18**, 355707 (2007).
[12] D. Calestani, M. Zha, A. Zappettini, L. Lazzarini, and L. Zanotti, Chem. Phys. Lett. **445**, 251 (2007).
[13] A. Othonos, J. Appl. Phys. **83**, 1789 (1998).
[14] X. C. Wu, J. M. Hong, Z. J. Han, and Y. R. Tao, Chem. Phys. Lett. **373**, 28 (2003).
[15] X. S. Peng, G. W. Meng, J. Zhang, X. F. Wang, Y. W. Wang, C. Z. Wang, and L. D. Zhang, J. Mater. Chem. **12**, 1602 (2002).
[16] X. S. Peng, Y. W. Wang, J. Zhang, X. F. Wang, L. X. Zhao, G. W. Meng, and L. D. Zhang, Appl. Phys. A: Mater. Sci. Process. **74**, 437 (2002).
[17] L. Dai, X. L. Chen, J. K. Jian, M. He, T. Zhou, and B. Q. Hu, Appl. Phys. A: Mater. Sci. Process. **75**, 687 (2002).
[18] J. Zhang, X. Qing, F. Jiang, and Z. Dai, Chem. Phys. Lett. **371**, 311 (2003).
[19] S. Q. Li, X. Y. Liang, C. Wang, X. Q. Fu, and T. H. Wang, Appl. Phys. Lett. **88**, 163111 (2006).
[20] Y. X. Liang, S. Q. Loi, L. Nie, Y. G. Wang, and T. H. Wang, Appl. Phys. Lett. **88**, 193119 (2006).
[21] M. Zervos, D. Tsokkou, M. Pervolaraki, and A. Othonos, Nanoscale Res. Lett. **4**, 491 (2009).
[22] M. Kumar, V. N. Singh, F. Singh, K. V. Lakshmi, B. R. Mehta, and J. P. Singh, Appl. Phys. Lett. **92**, 171907 (2008).
[23] A. Devizis, V. Vaicikauskas, and V. Gulbinas, Appl. Opt. **45**, 2535 (2006).
[24] S. Link, C. Burda, Z. L. Wang, and M. A. El-Sayed, J. Chem. Phys. **111**, 1255 (1999).
[25] T. S. Ahmadi, S. L. Logunov, and M. A. El-Sayed, J. Phys. Chem. **100**, 8053 (1996).
[26] M. Wraback, H. Shen, V. Sampath, C. J. Collins, G. A. Garrett, and W. L. Sarney, Phys. Status Solidi A **202**, 790 (2005).
[27] S. Wu, P. Geiser, J. Jun, J. Karpinski, J. R. Park, and R. Sobolewski, Appl. Phys. Lett. **88**, 041917 (2006).
[28] C. Thomsen, H. T. Grahn, H. J. Maris, and J. Tauc, Phys. Rev. B **34**, 4129 (1986).
[29] B. R. Krishna, T. K. Subramanian, B. S. Nadia, and S. Ruthann, Opt. Mater. (Amsterdam, Neth.) **15**, 217 (2000).

Downloaded 30 May 2010 to 194.42.23.188. Redistribution subject to AIP license or copyright; see http://jap.aip.org/jap/copyright.jsp